



# Superior CO<sub>2</sub>, CH<sub>4</sub>, and H<sub>2</sub> uptakes over ultrahigh-surface-area carbon spheres prepared from sustainable biomass-derived char by CO<sub>2</sub> activation

Yang Li <sup>1</sup>, Dawei Li <sup>1</sup>, Yuan Rao, Xuebo Zhao, Mingbo Wu\*

State Key Laboratory of Heavy Oil Processing, China University of Petroleum (East China), Qingdao, 266580, China

## ARTICLE INFO

### Article history:

Received 15 February 2016  
Received in revised form  
13 April 2016  
Accepted 15 April 2016  
Available online 16 April 2016

## ABSTRACT

Porous carbon spheres (PCSs) with high uptakes for CO<sub>2</sub>, CH<sub>4</sub>, and H<sub>2</sub> were prepared from sustainable starch-derived hydrochar via a simple CO<sub>2</sub> activation without any template. The PCSs show regularly-spherical morphology, large surface area (3350 m<sup>2</sup>/g), and high pore volume (1.75 ml/g), which have been rarely reported for physically-activated carbons. Owing to the textural properties, their uptakes at 20 bar for CO<sub>2</sub> (21.2 mmol/g, 298 K), CH<sub>4</sub> (10.7 mmol/g, 298 K), and H<sub>2</sub> (6.4 wt%, 77 K) all rank among the highest values ever reported for activated carbons, and the CH<sub>4</sub> uptake is the highest one for activated carbons. Additionally, the adsorption and desorption of the aforementioned gases onto the material are reversible, indicating that the PCSs can be regenerated readily by pressure swing adsorption. Given the sustainability and environmental friendliness of the starch-derived feedstock, low costs of physical activation, large uptakes for multiple gases, and excellent adsorption reversibility, the obtained PCSs are promising candidates for storage of multiple energy-source-related gases.

© 2016 Elsevier Ltd. All rights reserved.

## 1. Introduction

Carbon dioxide is the major greenhouse gas causing global warming and anthropogenic climate change [1]. Unfortunately, its atmospheric concentration remains increasing, mainly due to the large-scale burning of fossil fuels in emission sources like power plants. To reduce the emission of CO<sub>2</sub>, it is highly necessary to develop technologies for CO<sub>2</sub> capture and storage. The Intergovernmental Panel on Climate Change has estimated that the CO<sub>2</sub> emission could be reduced by 80–90% for a modern power plant equipped with CO<sub>2</sub> capture and storage technologies [2]. Besides these technologies, the emission of CO<sub>2</sub> can be decreased by using low-carbon energy sources, such as CH<sub>4</sub> and H<sub>2</sub>. One of the major concerns of this route is to find technologies that can efficiently store the energy-source-related gases.

Adsorption is applicable to both gas capture and storage. So far, many adsorbents have been developed, such as zeolites, porous silica, metal-organic frameworks, porous polymers, and porous carbons [1,3]. Among them, spherical porous carbons have received

much attention, due to their high surface-to-volume ratio, good structural stability, low regeneration energy, and large void space for encapsulating plenty of guests [4–6].

For example, Yu et al. prepared N-doped porous carbon hollow sphere with a CO<sub>2</sub> uptake of 4.42 mmol/g (273 K, 1 bar) by using melamine-formaldehyde nanosphere as a hard template and resorcinol-formaldehyde resin as a carbon precursor [7]. Bingjun et al. synthesized activated carbon spheres for CO<sub>2</sub> capture from poly(acrylonitrile-co-acrylamide) by KOH activation [8]. Alabadi et al. found that the porous carbons prepared from gelatin-starch mixture by KOH activation exhibited a CO<sub>2</sub> uptake of 7.49 mmol/g (1 bar, 273 K) [9]. Choma et al. reported that KOH-activated spherical porous carbons prepared from sulphonated styrene divinylbenzene resin displayed a CH<sub>4</sub> uptake of 1.68 mmol/g at 293 K and 1.1 bar [10]. Sevilla et al. manufactured an activated carbon sphere with a H<sub>2</sub> uptake of 6.4wt% (20 bar, 77 K) by KOH activation of hydrothermally-carbonized organic materials (furfural, glucose, etc.) [11]. In a word, previous works have showed that porous carbon spheres (PCSs) are promising adsorbents for energy-source-related gases such as CO<sub>2</sub>, CH<sub>4</sub>, and H<sub>2</sub>. Nevertheless, the preparation of these PCSs for gas adsorption frequently needs unsustainable/toxic feedstocks, harsh activators like KOH, and/or plenty of templates, which are undesirable both

\* Corresponding author.

E-mail address: [wumb@upc.edu.cn](mailto:wumb@upc.edu.cn) (M. Wu).

<sup>1</sup> The two authors contribute equally to this work.

economically and environmentally.

Hence, this research aims to prepare PCSs for efficient adsorption of CO<sub>2</sub>, CH<sub>4</sub>, and H<sub>2</sub> from a sustainable biomass (starch) by environment-friendly CO<sub>2</sub> activation without any template. Starch was previously used to produce carbon spheres with specific surface areas less than 2600 m<sup>2</sup>/g for supercapacitors [12–15]. In this research, we prepare starch-based PCSs with regularly-spherical morphology, large specific surface area (3350 m<sup>2</sup>/g), and high pore volume (1.75 ml/g), which have been rarely reported for physically-activated carbons. Moreover, the uptakes of the material at 20 bar for CO<sub>2</sub> (21.2 mmol/g, 298 K), CH<sub>4</sub> (10.7 mmol/g, 298 K), and H<sub>2</sub> (6.4wt%, 77 K) all rank among the highest values ever reported for activated carbons, and the CH<sub>4</sub> uptake is the highest one recorded for activated carbons.

## 2. Experimental section

### 2.1. Preparation of spherical porous carbons

To prepare PCSs, firstly, 15 g starch (AR, Sinopharm Chemical Reagent Co.,Ltd.) dissolving in 50 ml water was heated up to 353 K for gelatinization. The resulting pasty product was transferred into a stainless steel autoclave, heated up to 463 K in an oven, and kept at this temperature for 720 min. The obtained product was washed with distilled water and ethanol (AR, Sinopharm Chemical Reagent Co.,Ltd.), and then dried at 373 K for 360 min to yield carbon spheres recorded as CSs. Subsequently, the CSs were heated in a tube furnace under flowing N<sub>2</sub> (60 ml/min, 99.9% purity) by heating at 5 K/min first to 773 K with a retention time of 180 min and then to 1273 K. When the 1273 K was reached, flowing CO<sub>2</sub> (100 ml/min, 99.9% purity) was introduced to activate the sample for 150 min. Finally, the activated sample was cooled naturally to room temperature in N<sub>2</sub> flow (60 ml/min). The obtained PCSs were recorded as M1273-150, where 1273 and 150 denoted activation temperature (K) and activation time (min), respectively. The yield of M1273-150, which was defined as the weight ratio of final sample to the starting starch, was 2.1%.

### 2.2. Characterizations

X-ray diffraction (XRD) patterns of materials were obtained on an X-ray diffractometer (X'Pert PRO MPD, Netherlands) operating at 40 mA and 40 kV using Cu K $\alpha$  radiation. Surface morphology was observed by a scanning electron microscopy (SEM, S4800, Japan) operating at an acceleration voltage of 5.0 kV. Nitrogen adsorption/desorption isotherms of samples were measured by a volumetric adsorption analyser (Micromeritics, ASAP 2020, USA) after the samples were degassed under vacuum at 573 K for 6 h. The specific surface area ( $S_{\text{BET}}$ ) and total pore volume ( $V_t$ ) were obtained using the Brunauer–Emmett–Teller (BET) equation and the liquid volume of N<sub>2</sub> adsorbed at a relative pressure of 0.98, respectively. The pore size distribution and ultramicropore volume ( $V_{<0.7\text{nm}}$ ) were both determined by employing the Density Functional Theory (DFT, slit pore geometry) provided by the software of Micromeritics Corporation. The micropore volumes, namely  $V_{\text{micro-tplot}}$  and  $V_{\text{micro-DA}}$ , were derived via *t*-plot method [16] and Dubinin–Astakhov equation, respectively, and so were the micropore surface areas ( $S_{\text{micro-tplot}}$  and  $S_{\text{micro-DA}}$ ).

The Fourier transform infrared (FTIR) spectra in the wave-number range of 500–4000 cm<sup>−1</sup> were recorded using a Nicolet 6700 FTIR instrument (Nexus, USA) with a KBr pellet method. The activation burn-off was obtained via dividing the CO<sub>2</sub>-activation-induced weight loss by the weight of the carbon spheres heated to 1273 K. The O/C molar ratio of M1273-150 was determined by an X-ray photoelectron spectroscopy (XPS, K-Alpha, Thermo Scientific

Corp., USA) equipped with an Al K $\alpha$  X-ray source (1486.6 eV). The binding energies for the XPS spectrum were calibrated by setting C1s to 284.6 eV.

### 2.3. Gas adsorption measurements

The adsorption/desorption isotherms for CO<sub>2</sub>, CH<sub>4</sub>, and H<sub>2</sub> were measured using an intelligent gravimetric analyser (IGA, Hiden, UK) at different temperatures (273–313 K) and pressures (up to 20 bar), with the adsorption results corrected by buoyancy effects using the corrected parameters reported [17,18]. The microbalance contained in the analyser can measure weight with a resolution of  $\pm 0.1$   $\mu$ g. The purity of the used CO<sub>2</sub>, CH<sub>4</sub>, and H<sub>2</sub> was 99.999%, 99.999%, and 99.9999%, respectively. Before adsorption measurements, samples were degassed under 10<sup>−6</sup> bar at 473 K for 5 h. The isosteric heats of adsorption were calculated using the Clausius–Clapeyron equation and the adsorption isotherms at different temperatures, as reported previously [19].

## 3. Results and discussion

### 3.1. Characterizations

**Fig. 1** shows the SEM images of the obtained samples. The high-temperature-activated PCSs (M1273-150) are regularly-spherical and crack-free (**Fig. 1c** and **d**), as in the case of the inactivated carbon spheres (CSs, **Fig. 1a** and **b**). This observation indicates that the CSs are thermally and morphologically stable, and hence their spherical morphology is retained after high-temperature activation. The average particle sizes of M1273-150 are lower than those of CSs (**Fig. 1c** and **a**), which was probably attributable to the skeleton shrinkage of CSs or the removal of chemical elements (C, O, etc.) from CSs during activation.

The XRD pattern of M1273-150 (**Fig. 2**) exhibits a broad peak, implying that M1273-150 consists of amorphous carbons with a low graphitization degree. The FTIR spectra of CSs and M1273-150 are presented in **Fig. 3a**. The CSs display absorption bands attributable to C–O (1023 and 1213 cm<sup>−1</sup>) [20,21], C=O (1622 and 1720 cm<sup>−1</sup>) [22], and O–H (3421 cm<sup>−1</sup>) [20,23]. In contrast, M1273-150 shows no/a few weak absorption bands at the corresponding wave numbers, indicating that most O-containing functional groups have been removed after activation. The analysis of XPS spectrum (**Fig. 3b**) shows that the O/C molar ratio for M1273-150 is low (3.2%), which further proves the removal of most O-containing function groups from this sample.

The adsorption–desorption isotherms of M1273-150 are presented in **Fig. 4**. The isotherms feature a N<sub>2</sub>-uptake increment up to a relative pressure of 0.4, an adsorption plateau, and no hysteresis loop, indicating that they are type I<sub>b</sub> isotherms [24]. Such isotherms have been reported for physically-activated carbons with high burn-offs [24]. In the case of M1273-150, the burn-off is as high as 90.1%. These isotherms indicate that M1273-150 is microporous, with the presence of narrow mesopores. **Table 1** shows that M1273-150 has a large micropore surface area, as revealed by  $S_{\text{micro-tplot}}$  and  $S_{\text{micro-DA}}$ , and a high micropore volume, as indicated by  $V_{\text{micro-tplot}}$  and  $V_{\text{micro-DA}}$ . These observations also prove that M1273-150 has plenty of micropores. The micropore size concentrates in a narrow range (0.50–0.80 nm and 1.18–1.52 nm), and so does the mesopore size (2–4 nm, see inset in **Fig. 4**). It should be mentioned that the DFT-derived pore size distribution can underestimate the micropore volume for the following two reasons. Firstly, the used DFT method causes an artificial minimum at around 1 nm, due to the modelling assumptions [24,25]. Secondly, some ultramicropores (<0.7 nm) are inaccessible to N<sub>2</sub> molecules at 77 K [26], due to diffusion limitations.

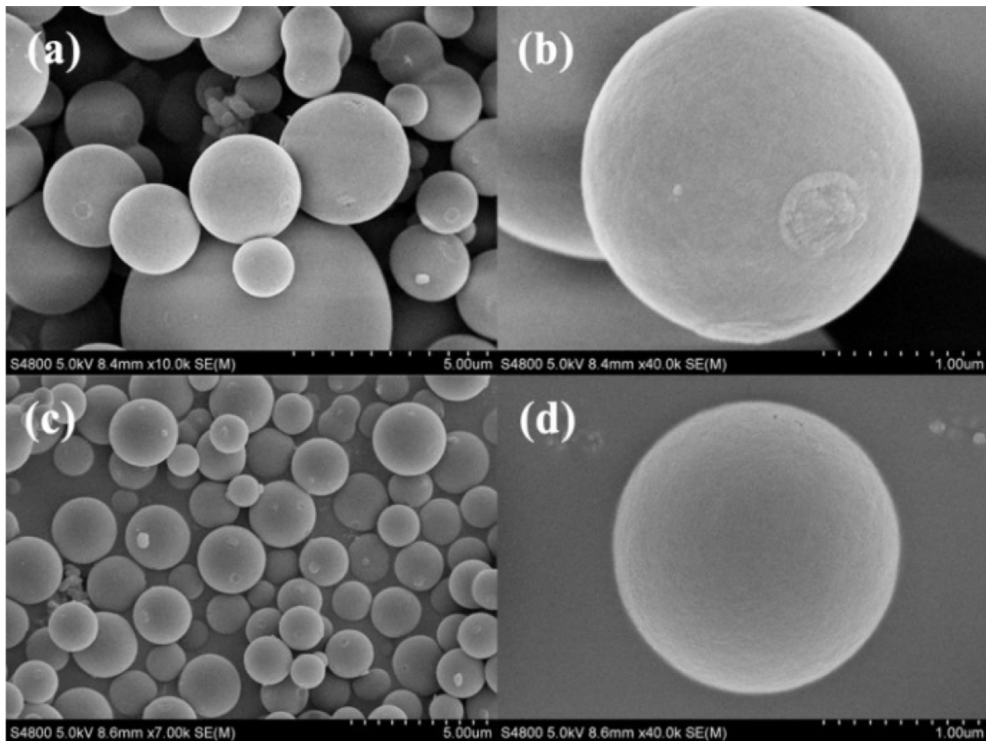


**Fig. 1.** SEM images for carbon spheres (CSs) at magnifications of (a) 10,000 and (b) 40,000, and for porous carbon spheres (M1273-150) at magnifications of (c) 7000 and (d) 40,000.

Additionally, Table 1 shows that M1273-150 displays simultaneously a large specific surface area ( $3350 \text{ m}^2/\text{g}$ ) and a high pore volume (1.75 ml/g), which are rarely-reported textural properties for porous carbons prepared via  $\text{CO}_2$  activation. The formation of such textural properties is attributable to the creation of new micropores, the opening of closed pores, or the widening of pre-existent pores caused by devolatilization and carbon- $\text{CO}_2$  reaction [21]. To gain further insight into the explanations, we produced a carbonized carbon sphere (C1273-150) in the same way that M1273-150 was prepared, except that C1273-150 was heated at 1273 K in flowing  $\text{N}_2$  (100 ml/min) instead of  $\text{CO}_2$ . It is found that the  $S_{\text{BET}}$  and  $V_t$  of C1273-150 (401  $\text{m}^2/\text{g}$  and 0.17 ml/g) are much lower than the corresponding values of M1273-150 (3350  $\text{m}^2/\text{g}$  and 1.75 ml/g), indicating that the developed pore structure of M1273-150 is mainly due to the  $\text{CO}_2$  activation which

causes a high burn-off (90.1%). Also, it is found that (1) the  $S_{\text{BET}}$  and  $V_t$  of C1273-150 (401  $\text{m}^2/\text{g}$  and 0.17 ml/g) are higher than the

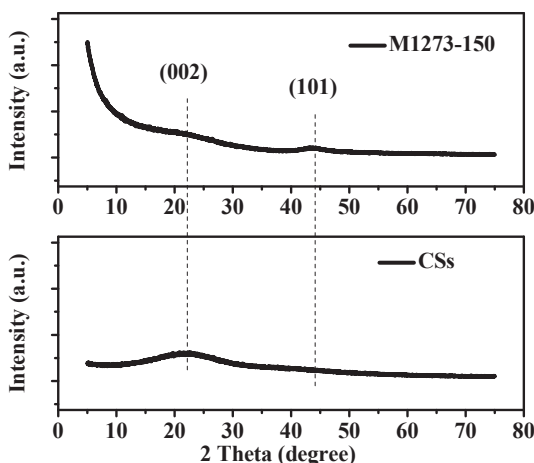


**Fig. 2.** XRD patterns of carbon spheres (CSs) and porous carbon spheres (M1273-150).

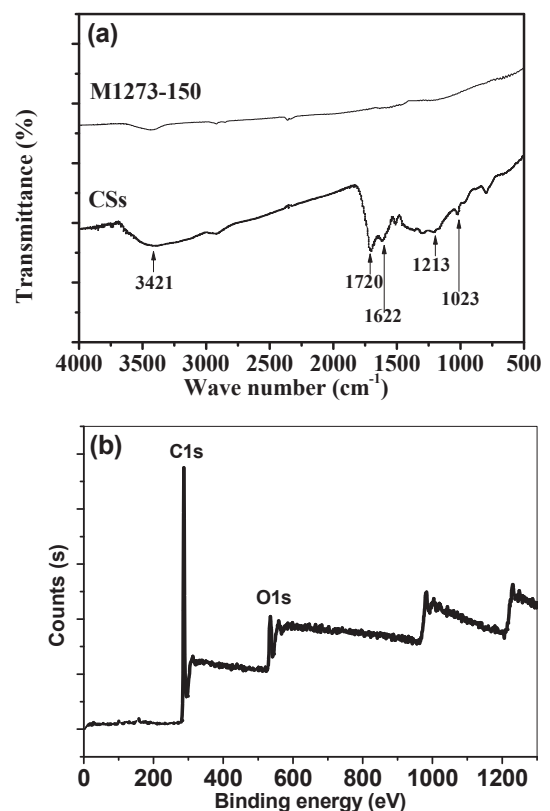


**Fig. 3.** (a) FTIR spectra for carbon spheres (CSs) and porous carbon spheres (M1273-150), and (b) XPS spectrum for M1273-150.

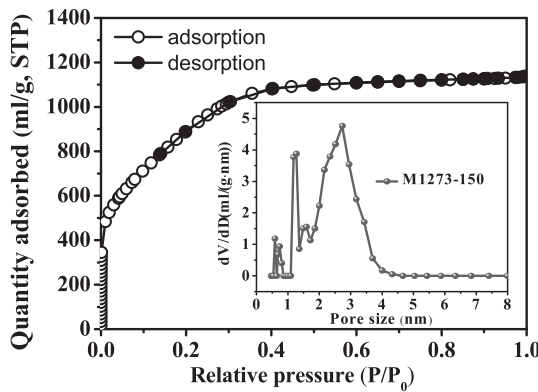


**Fig. 4.**  $\text{N}_2$  adsorption–desorption isotherms and pore size distribution (inset) of M1273-150.

**Table 1**  
Textural properties of M1273-150.

| $S_{\text{BET}}$<br>( $\text{m}^2/\text{g}$ ) | $S_{\text{micro-tplot}}$<br>( $\text{m}^2/\text{g}$ ) | $S_{\text{micro-DA}}$<br>( $\text{m}^2/\text{g}$ ) | $V_t$<br>(ml/g) | $V_{\text{micro-tplot}}$<br>(ml/g) | $V_{\text{micro-DA}}$<br>(ml/g) | $V_{<0.7\text{nm}}$<br>(ml/g) | $V_{\text{micro-tplot}}/V_t$ (%) | $V_{\text{micro-DA}}/V_t$ (%) |
|---|---|--|-----------------|------------------------------------|---------------------------------|-------------------------------|----------------------------------|-------------------------------|
| 3350  | 3281  | 2330   | 1.75            | 1.67                               | 1.10                            | 0.08                          | 95.4                             | 62.9                          |

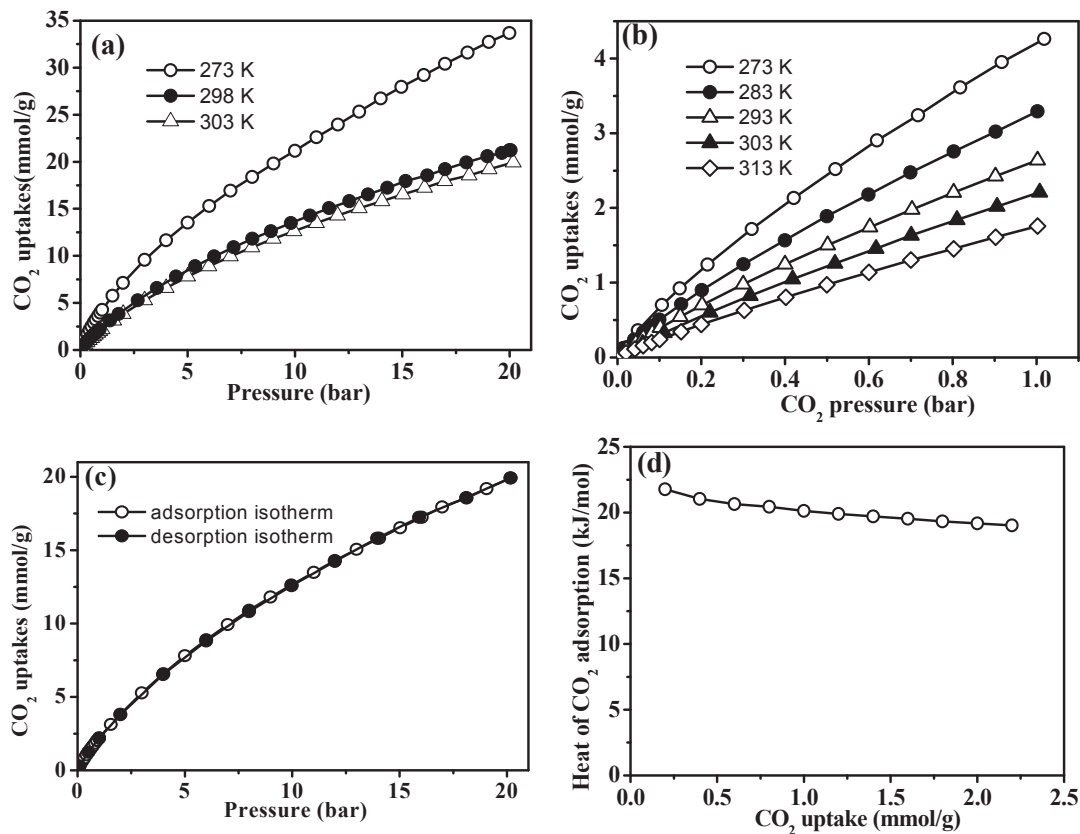


**Fig. 5.**  $\text{CO}_2$  adsorption performance of M1273-150. (a) adsorption isotherms at pressures up to 20 bar, (b) adsorption isotherms in pressure range of 0–1 bar, (c) adsorption reversibility at 303 K, and (d) heat of adsorption.

corresponding ones of the carbon spheres (CSs,  $<20 \text{ m}^2/\text{g}$  and  $<0.03 \text{ ml/g}$ ) and (2) the weight ratio of C1273-150 to the CSs is 70%. These observations suggest that the heat-treatment-induced devolatilization of CSs also contributes to the increase in  $S_{\text{BET}}$  and  $V_t$ .

### 3.2. Adsorption performance for $\text{CO}_2$

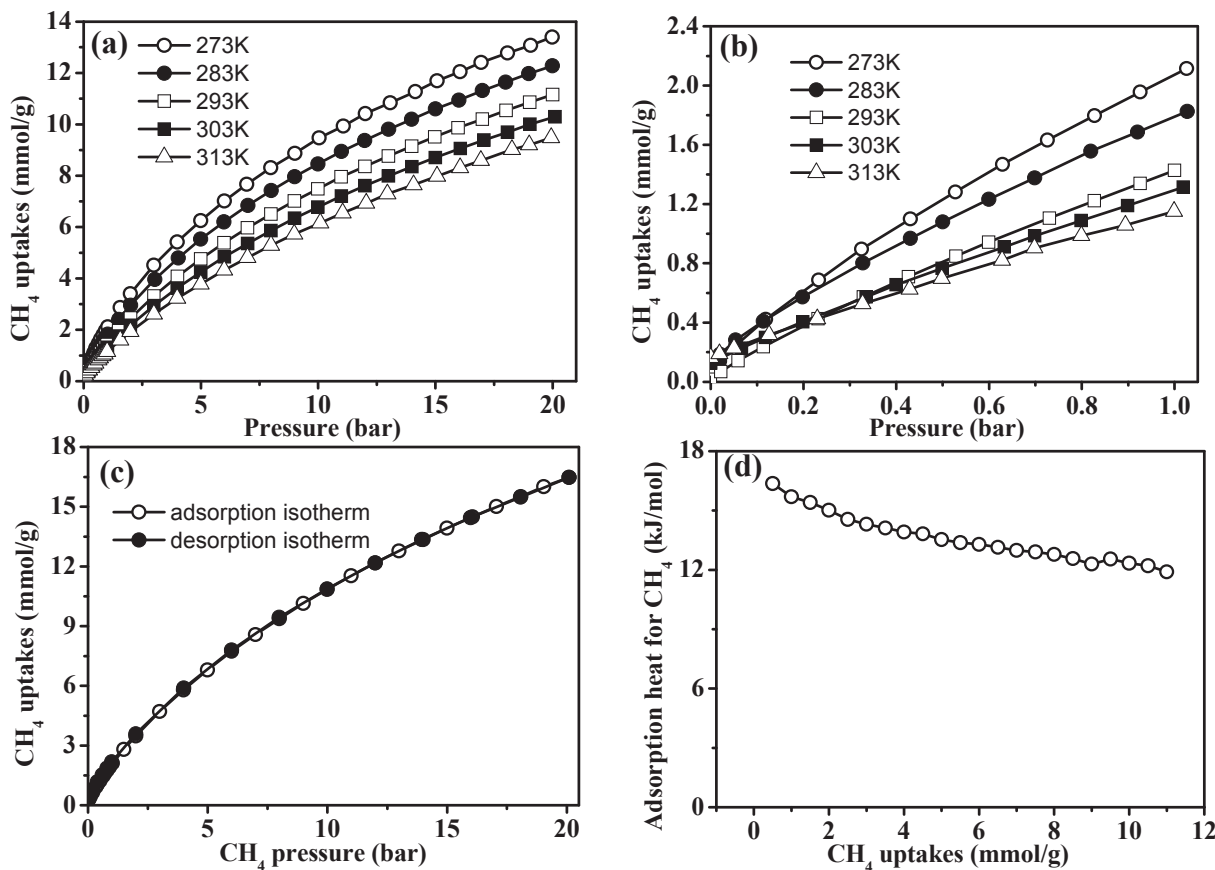
The  $\text{CO}_2$  adsorption isotherms of M1273-150 are presented in Fig. 5a and b. The  $\text{CO}_2$  uptake increases with the increment in adsorption pressure, not levelling off at the highest test pressure (20 bar). This result suggests that a greater  $\text{CO}_2$  uptake can be achieved at a higher adsorption pressure. Typical  $\text{CO}_2$  uptakes derived from Fig. 5a are provided in Table 2. The  $\text{CO}_2$ -activated M1273-150 exhibits a  $\text{CO}_2$  uptake of 21.2 mmol/g at 20 bar and 298 K, ranking among the highest values ever reported for activated carbons including KOH-activated ones (Table 2). M1273-150 also exhibits large  $\text{CO}_2$  uptakes at other pressures (14, 10, or 5 bar), compared with MOFs, zeolites, and templated carbons (Table 2). These results indicate that M1273-150 possesses a strong ability to store  $\text{CO}_2$  at high pressures. The strong ability to adsorb  $\text{CO}_2$  at high pressures ( $\geq 10$  bar) is ascribable to the large specific surface area

and multiple pores of porous carbons, as reported previously [27–30]. Hence, M1273-150, which possesses a high  $S_{\text{BET}}$  (Table 1), a considerable  $V_{\text{micro}}$  (Table 1), and a fraction of mesopores (inset in Fig. 4), can adsorb plenty of  $\text{CO}_2$  at high pressures.

Fig. 5c shows that the adsorption and desorption isotherms

**Table 2**High-pressure CO<sub>2</sub> uptakes at 298 K.

| Adsorbent <sup>a</sup>   | Preparation method                        | CO <sub>2</sub> uptake <sup>b</sup><br>(mmol/g) | Reference        |
|--|---|---|------------------|
| Carbonaceous adsorbents (below)  |   |   |                  |
| <b>Starch-based PC(M1273-150)</b>  | <b>CO<sub>2</sub> activation</b>          | <b>21.2 (20 bar)</b>                            | <b>This work</b> |
|  | <b>CO<sub>2</sub> activation</b>          | <b>17.0 (14 bar)</b>                            | <b>This work</b> |
|  | <b>CO<sub>2</sub> activation</b>          | <b>13.7 (10 bar)</b>                            | <b>This work</b> |
|  | <b>CO<sub>2</sub> activation</b>          | <b>8.5 (5 bar)</b>                              | <b>This work</b> |
| Poly(vinylidene chloride)-based PC(AC4-PC)                                       | KOH activation                            | 18.3 (20 bar)                                   | [17]             |
| Anther-based PC(PA-500-KOH-4-800)  | KOH activation                            | -21.6 (20 bar)                                  | [31]             |
| Petroleum residue –based PC(VR5-4:1)   | KOH activation                            | 21.6 (20 bar)                                   | [28]             |
| Porous benzimidazole-linked polymer-based PC(CPC-700)                            | KOH activation                            | -21.1 (20 bar)                                  | [32]             |
| Algae meal-based PC(AMA-C-KOH)   | KOH activation                            | <14.0 (20 bar)                                  | [33]             |
| Ion exchange resin-based PC(MCK-3)   | KOH activation                            | -17.5 (14 bar)                                  | [30]             |
| Coal tar pitch-based PC(ACB-5)   | KOH activation                            | -17.6 (14 bar)                                  | [34]             |
| Petroleum coke-based PC(K4-90@200-60@700-150-5)                                  | KOH activation                            | 8.4 (10 bar)                                    | [29]             |
| Palm shell-based PC(MCa2)  | CaCl <sub>2</sub> activation              | -11.5 (20 bar)                                  | [35]             |
| Palm shell-based PC(MZn48)   | ZnCl <sub>2</sub> activation              | -8.5 (20 bar)                                   | [35]             |
| Palm shell-based PC(MP48)  | H <sub>3</sub> PO <sub>4</sub> activation | -7.8 (20 bar)                                   | [35]             |
| Exchange resin –based PC(AM4)  | MgO templating                            | <18.2 (20 bar)                                  | [36]             |
| Commercial PC(Norit R1Extra)   | Unreported                                | <9.7 (20 bar)                                   | [37]             |
| Commercial PC(Maxsorb)   | Unreported                                | <20.0 (20 bar)                                  | [37]             |
| Amine-grafted commercial PC  | Unreported                                | <3.5 (10 bar)                                   | [38]             |
| Exchange resin –based PC(AM4)  | MgO templating                            | <12.0 (10 bar)                                  | [36]             |
| K <sub>2</sub> CO <sub>3</sub> -modified PC(K <sub>2</sub> CO <sub>3</sub> /MAC) | Unreported                                | <1.4 (5 bar)                                    | [19,39]          |
| Non-carbonaceous adsorbents (below)  |   |   |                  |
| Zr-MOF (UiO-66)  | No activation                             | <7.0 (20 bar)                                   | [40]             |
| MOF-5  | No activation                             | 10.9 (14 bar)                                   | [41]             |
| MOF-177  | No activation                             | 2.0 (14 bar)                                    | [41]             |
| Zeolite 5A   | No activation                             | 5.1 (14 bar)                                    | [41]             |
| Zeolite 13X  | No activation                             | <7.0 (10 bar)                                   | [42]             |

<sup>a</sup> PC and character strings in parentheses denoted porous carbon and reported sample names, respectively.<sup>b</sup> The numbers in parentheses were adsorption pressures.**Fig. 6.** CH<sub>4</sub> adsorption performance of M1273-150. (a) adsorption isotherms at pressures up to 20 bar, (b) adsorption isotherms in pressure range of 0–1 bar, (c) adsorption reversibility at 303 K, and (d) heat of adsorption.

**Table 3**CH<sub>4</sub> uptakes of various adsorbents at temperatures around 298 K.

| Adsorbent <sup>a</sup>  | Preparation method                                    | CH <sub>4</sub> uptake <sup>b</sup><br>(mmol/g) | Reference        |
|---|---|---|------------------|
| CH <sub>4</sub> uptakes at 20 bar and 298 K (below)                         |   |   |                  |
| <b>Starch-based PC(M1273-150)</b>   | <b>CO<sub>2</sub> activation</b>                      | <b>10.7</b>                                     | <b>This work</b> |
| Algae meal-based PC(AMA-C-KOH)  | KOH activation  | <7.5  | [33]             |
| Poly(vinylidene chloride)-based PC (AC4-PC)                                 | KOH activation  | 10.3  | [17]             |
| Porous benzimidazole-linked polymer-based PC(CPC-700)                       | KOH activation  | <10.1   | [32]             |
| Mesophase pitch(LMA738)   | KOH activation  | <9.4  | [44]             |
| Palm shell-based PC(MP48)   | H <sub>3</sub> PO <sub>4</sub> activation             | -3.8  | [35]             |
| Olive stone –based PC(ACP-410)  | H <sub>3</sub> PO <sub>4</sub> activation             | -4.5  | [45]             |
| Palm shell-based PC(MCa2)   | CaCl <sub>2</sub> activation                          | -5.8  | [35]             |
| Palm shell-based PC(MZn48)  | ZnCl <sub>2</sub> activation                          | -3.9  | [35]             |
| Coal-based PC(S-800-90-12)  | K <sub>2</sub> S activation                           | -3.8  | [43]             |
| Coconut shell-based PC(M40-28)  | Activation with ZnCl <sub>2</sub> and CO <sub>2</sub> | <3.3  | [46]             |
| Polymer-based PC(DUT-38-A-950-4)  | CO <sub>2</sub> activation                            | -9.4  | [47]             |
| Peat-based PC(RB3)  | Steam activation                                      | <4.5  | [48]             |
| Peat-based commercial PC(Norit R1 Extra)                                    | Unreported  | <5.5  | [37]             |
| Chark-based commercial PC(Maxsorb)  | Unreported  | <9.5  | [37]             |
| Coconut shell-based PC (K835)   | Unreported  | <6.0  | [48]             |
| Resin-based carbon (CS)   | No activation   | -2.5  | [49]             |
| Zr-MOF(UiO-66)  | No activation   | <4.0  | [40]             |
| CH <sub>4</sub> uptakes under conditions except at 20 bar and 298 K (below) |   |   |                  |
| <b>Starch-based PC(M1273-150)</b>   | <b>CO<sub>2</sub> activation</b>                      | <b>10.3 (20bar, 303 K)</b>                      | <b>This work</b> |
|   | <b>CO<sub>2</sub> activation</b>                      | <b>7.2 (10bar, 298 K)</b>                       | <b>This work</b> |
| Corn grain-based PC (MR-1/4-CMC-5%)   | KOH activation  | <9.8 (20bar, 303 K)                             | [50]             |
| Glucose-based PC(G3-950-3)  | Zeolite-templating                                    | <6.5 (20bar, 300 K)                             | [51]             |
| Coal tar pitch-based PC(ACB-5)  | KOH activation  | ~6.9 (10bar, 298 K)                             | [34]             |

<sup>a</sup> PC and character strings in parentheses meant porous carbon and reported sample names, respectively.<sup>b</sup> The numbers in parentheses were adsorption pressures and temperatures.

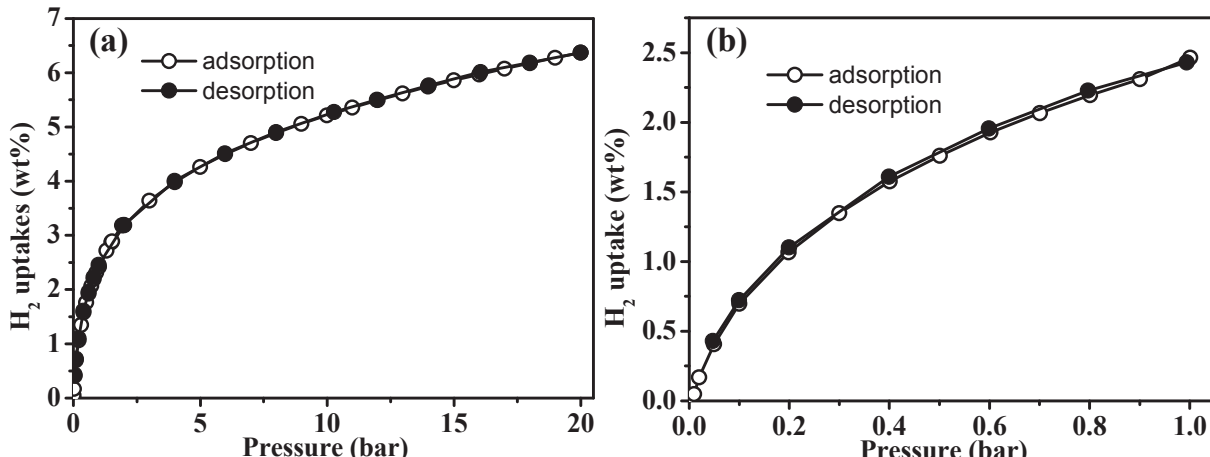
overlap, indicating that the CO<sub>2</sub> adsorption on the sample is completely reversible and that the adsorbent can be readily regenerated by reducing adsorption pressure. Fig. 5d shows that the CO<sub>2</sub> adsorption heat (20–25 kJ/mol) of M1273-150 is lower than the typical value for chemisorption (>60 kJ/mol) [3], confirming that the CO<sub>2</sub> molecules are physically adsorbed onto the sample. Given the moderate adsorption heat, good reversibility, and large uptakes, the M1273-150 is an excellent adsorbent for CO<sub>2</sub> storage.

### 3.3. Adsorption performance for CH<sub>4</sub>

The CH<sub>4</sub> adsorption isotherms of M1273-150 are presented in Fig. 6 a and b. The isotherm becomes lower as the adsorption temperature increases, due to the exothermic nature of the adsorption. Typical CH<sub>4</sub> uptakes derived from the isotherms are

presented in Table 3. The CH<sub>4</sub> uptake of the sample reaches 10.7 mmol/g at 20 bar (298 K), which, to the best of our knowledge, is an unprecedentedly reported value for activated carbons. For instance, the uptake of this CO<sub>2</sub>-activated sample exceeds those of KOH-activated carbons, H<sub>3</sub>PO<sub>4</sub>-activated carbons, and the commercial activated carbon Maxsorb (Table 3). The superior CH<sub>4</sub> uptakes at high pressures are ascribable to the large specific surface area and considerable micropore volume of M1273-150 (Table 1), as revealed previously [17,43]. The narrow micropore and mesopore size distributions of the material (inset in Fig. 4) are also probable reasons for the high CH<sub>4</sub> uptakes. These high uptakes indicate that the obtained material is a promising adsorbent for CH<sub>4</sub> storage.

Besides high CH<sub>4</sub> uptakes, M1273-150 also exhibits good adsorption reversibility, as indicated by the overlapped adsorption/desorption isotherms (Fig. 6c). Fig. 6d shows that the adsorption

Fig. 7. H<sub>2</sub> adsorption isotherms for M1273-150 at 77 K in pressure range of (a) 0–20 bar, and (b) 0–1 bar.

**Table 4**H<sub>2</sub> uptakes of carbonaceous adsorbents at 77 K.

| Porous carbon <sup>a</sup>   | Preparation method                | H <sub>2</sub> uptake at 20 bar or 1 bar (wt%) | Reference        |
|--|-----------------------------------|--|------------------|
| H <sub>2</sub> uptake at 20 bar (below)                              |                                   |  |                  |
| <b>Starch-based PC(M1273-150)</b>                                    | <b>CO<sub>2</sub> activation</b>  | <b>6.4</b>                                     | <b>This work</b> |
| Polymer-based PC(DUT-38-A-950-4)                                     | CO <sub>2</sub> activation        | <5.5   | [47]             |
| Cellulose-based PC(AC1 (1/4-700))                                    | KOH activation                    | 6.4  | [11]             |
| Sawdust-based PC(E-1/4-700)  | KOH activation                    | 5.6  | [11]             |
| Anthracite-based PC(AC6)   | KOH activation                    | 5.2  | [54]             |
| Fungi-based PC(AG-4-700)   | KOH activation                    | <5   | [55]             |
| Corncob-derived PC(CAC-4)  | KOH activation                    | <5.5   | [56]             |
| PdCl <sub>2</sub> <sup>+</sup> -exchanged resin-based PC (Pd/PC-850) | KOH activation                    | 4.6  | [57]             |
| Chitosan-based PC (Ch700/700/3)                                      | KOH activation                    | <5.6   | [58]             |
| Coal-based porous carbon (B704)                                      | KOH activation                    | <6.3   | [59]             |
| Anthracite-derived PC  | KOH activation                    | <6.0   | [60]             |
| Biomass-cartons-polystyrene mixture-based PC(AC)                     | ZnCl <sub>2</sub> activation      | <2.5   | [61]             |
| Acetonitrile-based PC  | SBA-15-templating                 | 3.4  | [62]             |
| Furfuryl alcohol and acetylene (10Xc-70)                             | Zeolite-templating                | 6.1  | [18]             |
| Furfuryl alcohol-based PC (AC-BF900@5TON)                            | ZIF-templating and KOH activation | 6.5  | [63]             |
| Furfuryl alcohol-based PC (FA-ZTC1)                                  | Zeolite-templating and CVD        | 7.3  | [64]             |
| H <sub>2</sub> uptake at 1 bar (below)                               |                                   |  |                  |
| <b>Starch-based PC(M1273-150)</b>                                    | <b>CO<sub>2</sub> activation</b>  | <b>2.3</b>                                     | <b>This work</b> |
| Hemp stem-based PC(AC8)  | KOH activation                    | 3.3  | [52]             |
| Cellulose-based PC(AC1 (1/4-700))                                    | KOH activation                    | 2.5  | [11]             |
| Fungi-based PC(AG-4-700)   | KOH activation                    | 2.4  | [55]             |
| Sawdust-based PC(E-1/4-700)  | KOH activation                    | 2.5  | [11]             |
| Corn grain-based PC(MR-1/2)  | KOH activation                    | 2.3  | [65]             |
| Rice husk-based PC(RHC1)   | KOH activation                    | 2.9  | [66]             |
| Corncob-derived PC(CAC-4)  | KOH activation                    | 3.2  | [56]             |
| Alkene polymer-based PC(C-1012)                                      | Unreported                        | 2.2  | [67]             |

<sup>a</sup> PC and character strings in parentheses represented porous carbon and reported sample names, respectively.

heat ranges from 11 to 17 kJ/mol when the CH<sub>4</sub> uptake is in the range of 0.3–11 mmol/g, implying the occurrence of physisorption. Additionally, the adsorption heat decreases with the increase in CH<sub>4</sub> uptake, revealing that the sample surface is energetically heterogeneous for adsorption of CH<sub>4</sub>.

#### 3.4. Adsorption performance for H<sub>2</sub>

Fig. 7 shows the H<sub>2</sub> adsorption/desorption isotherms for M1273-150. The adsorption and desorption isotherms overlap, indicating that the adsorption of H<sub>2</sub> onto the sample is completely reversible. Table 4 displays the H<sub>2</sub> uptakes of M1273-150 at 20 bar and 1 bar. At 20 bar, the H<sub>2</sub> uptake (6.4 wt%, 77 K) of this CO<sub>2</sub>-activated sample prepared without any template is among the highest values ever reported for activated carbons including KOH-activated ones, and is comparable/superior to those of many templated carbons (Table 4). The H<sub>2</sub> adsorption onto porous carbons at high pressures is determined by specific surface area and pore volume (especially micropore volume), with the small mesopores (2–5 nm) also making important contributions [52,53]. Hence, M1273-150, which has a large specific surface area, a high micropore volume, and a fraction of small mesopores (2–4 nm, inset in Fig. 4), displays high H<sub>2</sub> uptakes. The large high-pressure H<sub>2</sub> uptake of M1273-150 is also attributable to its deficiency in O-containing functional groups as revealed by the FTIR and XPS analysis (Fig. 3), in that such groups can reduce the interaction between H<sub>2</sub> and carbon surface [11]. At 1 bar, the H<sub>2</sub> uptake of M1273-150 is relatively low (Table 4), suggesting that the adsorbed H<sub>2</sub> at a high pressure can be readily released by reducing adsorption pressure.

#### 4. Conclusions

In summary, PCSs for efficient adsorption of CO<sub>2</sub>, CH<sub>4</sub>, and H<sub>2</sub> were prepared by physical activation of starch-derived char without any template. The obtained PCSs exhibited a regularly-spherical morphology, a large specific surface area (3350 m<sup>2</sup>/g),

and a high pore volume (1.75 ml/g), which were rarely reported for physically-activated carbons. The uptakes of the sample at 20 bar for CO<sub>2</sub>, CH<sub>4</sub>, and H<sub>2</sub> reached 21.2 mmol/g (298 K), 10.7 mmol/g (298 K), and 6.4 wt % (77 K), respectively, which were all among the highest values ever reported for activated carbons. Besides, the adsorption of the gases onto the sample was reversible, guaranteeing the ease of regenerating the PCSs by reducing adsorption pressure. The obtained materials are highly promising adsorbents for storing energy-source-related gases, given the sustainability and environmental friendliness of the feedstock, low costs of physical activation, high uptakes for multiple gases, and excellent adsorption reversibility.

#### Acknowledgements

The authors acknowledge the financial supports provided by the National Natural Science Foundation of China (51372277), the Fundamental Research Funds for the Central Universities (15CX08005A), and Qingdao Science and Technology Project (15-9-1-61-jch).

#### References

- [1] J.Y. Wang, L. Huang, R.Y. Yang, Z. Zhang, J.W. Wu, Y.S. Gao, et al., Recent advances in solid sorbents for CO<sub>2</sub> capture and new development trends, Energy Environ. Sci. 7 (2014) 3478–3518.
- [2] J.R. Li, Y.G. Ma, M.C. McCarthy, J. Sculley, J.M. Yu, H.K. Jeong, et al., Carbon dioxide capture-related gas adsorption and separation in metal-organic frameworks, Coord. Chem. Rev. 255 (2011) 1791–1823.
- [3] A. Samanta, A. Zhao, G.K.H. Shimizu, P. Sarkar, R. Gupta, Post-combustion CO<sub>2</sub> capture using solid sorbents –a review, Ind. Eng. Chem. Res. 51 (2012) 1438–1463.
- [4] N.P. Wickramaratne, M. Jaroniec, Activated carbon spheres for CO<sub>2</sub> adsorption, ACS Appl. Mater. Interfaces 5 (2013) 1849–1855.
- [5] M. Sevilla, C. Falco, M.M. Titirici, A.B. Fuertes, High-performance CO<sub>2</sub> sorbents from algae, Rsc Adv. 2 (2012) 12792–12797.
- [6] S. Wang, W.C. Li, L. Zhang, Z.Y. Jin, A.H. Lu, Polybenzoxazine-based monodisperse carbon spheres with low-thermal shrinkage and their CO<sub>2</sub> adsorption properties, J. Mater. Chem. A 2 (2014) 4406–4412.
- [7] Y. Wang, H. Zou, S. Zeng, Y. Pan, R. Wang, X. Wang, et al., A one-step

- carbonization route towards nitrogen-doped porous carbon hollow spheres with ultrahigh nitrogen content for CO<sub>2</sub> adsorption, *Chem. Commun.* 51 (2015) 12423–12426.
- [8] B. Zhu, K. Li, J. Liu, H. Liu, C. Sun, C.E. Snape, et al., Nitrogen-enriched and hierarchically porous carbon macro-spheres - ideal for large-scale CO<sub>2</sub> capture, *J. Mater. Chem. A* 2 (2014) 5481–5489.
- [9] A. Alabadi, S. Razzaque, Y. Yang, S. Chen, B. Tan, Highly porous activated carbon materials from carbonized biomass with high CO<sub>2</sub> capturing capacity, *Chem. Eng. J.* 281 (2015) 606–612.
- [10] J. Choma, L. Osuchowski, A. Dziura, M. Marszewski, M. Jaroniec, Benzene and methane adsorption on ultrahigh surface area carbons prepared from sulphonated styrene divinylbenzene resin by KOH activation, *Adsorpt. Sci. Technol.* 33 (2015) 587–594.
- [11] M. Sevilla, A.B. Fuertes, R. Mokaya, High density hydrogen storage in super-activated carbons from hydrothermally carbonized renewable organic materials, *Energy Environ. Sci.* 4 (2011) 1400–1410.
- [12] S. Zhao, J. Xiang, C.Y. Wang, M.M. Chen, Characterization and electrochemical performance of activated carbon spheres prepared from potato starch by CO<sub>2</sub> activation, *J. Porous Mater.* 20 (2013) 15–20.
- [13] S. Zhao, C.Y. Wang, M.M. Chen, J.H. Sun, Mechanism for the preparation of carbon spheres from potato starch treated by NH<sub>4</sub>Cl, *Carbon* 47 (2009) 331–333.
- [14] X. Wang, H. Wang, Q. Dai, Q. Li, J. Yang, A. Zhang, et al., Preparation of novel porous carbon spheres from corn starch, *Colloids Surfaces Physicochem. Eng. Aspects* 346 (2009) 213–215.
- [15] H. Wang, Q. Dai, Q. Li, J. Yang, X. Zhong, Y. Huang, et al., Preparation of porous carbon spheres from porous starch, *Solid State Ionics* 180 (2009) 1429–1432.
- [16] M.B. Wu, Q.F. Zha, J.S. Qiu, Y.S. Guo, H.Y. Shang, A.J. Yuan, Preparation and characterization of porous carbons from pan-based preoxidized cloth by KOH activation, *Carbon* 42 (2004) 205–210.
- [17] J.J. Cai, J.B. Qi, C.P. Yang, X.B. Zhao, Poly(vinylidene chloride)-based carbon with ultrahigh microporosity and outstanding performance for CH<sub>4</sub> and H<sub>2</sub> storage and CO<sub>2</sub> capture, *ACS Appl. Mater. Interfaces* 6 (2014) 3703–3711.
- [18] J.J. Cai, L.J. Li, X.X. Lv, C.P. Yang, X.B. Zhao, Large surface area ordered porous carbons via nanocasting zeolite 10X and high performance for hydrogen storage application, *ACS Appl. Mater. Interfaces* 6 (2014) 167–175.
- [19] P. Ning, F.R. Li, H.H. Yi, X.L. Tang, J.H. Peng, Y.D. Li, et al., Adsorption equilibrium of methane and carbon dioxide on microwave-activated carbon, *Sep. Purif. Technol.* 98 (2012) 321–326.
- [20] A.H. El-Sheikh, A.P. Newman, H.K. Al-Daffae, S. Phull, N. Cresswell, Characterization of activated carbon prepared from a single cultivar of Jordanian olive stones by chemical and physicochemical techniques, *J. Anal. Appl. Pyrolysis* 71 (2004) 151–164.
- [21] T. Yang, A.C. Lua, Characteristics of activated carbons prepared from pistachio-nut shells by physical activation, *J. Colloid Interface Sci.* 267 (2003) 408–417.
- [22] Y.B. Tang, Q. Liu, F.Y. Chen, Preparation and characterization of activated carbon from waste ramulus mori, *Chem. Eng. J.* 203 (2012) 19–24.
- [23] M.B. Wu, P.P. Ai, M.H. Tan, B. Jiang, Y.P. Li, J.T. Zheng, et al., Synthesis of starch-derived mesoporous carbon for electric double layer capacitor, *Chem. Eng. J.* 245 (2014) 166–172.
- [24] F. Suarez-Garcia, J.I. Paredes, A. Martinez-Alonso, J.M.D. Tascon, Preparation and porous texture characteristics of fibrous ultrahigh surface area carbons, *J. Mater. Chem.* 12 (2002) 3213–3219.
- [25] J. Silvestre-Albero, A. Silvestre-Albero, F. Rodriguez-Reinoso, M. Thommes, Physical characterization of activated carbons with narrow microporosity by nitrogen (77.4 k), carbon dioxide (273 k) and argon (87.3 k) adsorption in combination with immersion calorimetry, *Carbon* 50 (2012) 3128–3133.
- [26] G. Sethia, A. Sayari, Comprehensive study of ultra-microporous nitrogen-doped activated carbon for CO<sub>2</sub> capture, *Carbon* 93 (2015) 68–80.
- [27] J.P. Marco-Lozar, M. Kunowsky, F. Suarez-Garcia, A. Linares-Solano, Sorbent design for CO<sub>2</sub> capture under different flue gas conditions, *Carbon* 72 (2014) 125–134.
- [28] M.E. Casco, M. Martinez-Escandell, J. Silvestre-Albero, F. Rodriguez-Reinoso, Effect of the porous structure in carbon materials for CO<sub>2</sub> capture at atmospheric and high-pressure, *Carbon* 67 (2014) 230–235.
- [29] X.P. Zhu, Y. Fu, G.S. Hu, Y. Shen, W. Dai, X. Hu, CO<sub>2</sub> capture with activated carbons prepared by petroleum coke and KOH at low pressure, *Water Air Soil Poll.* 224 (2013) 1387–1399.
- [30] L.Y. Meng, S.J. Park, MgO-templated porous carbons-based CO<sub>2</sub> adsorbents produced by KOH activation, *Mater. Chem. Phys.* 137 (2012) 91–96.
- [31] J. Song, W.Z. Shen, J.G. Wang, W.B. Fan, Superior carbon-based CO<sub>2</sub> adsorbents prepared from poplar anthers, *Carbon* 69 (2014) 255–263.
- [32] B. Ashourirad, A.K. Sekizkardes, S. Altarawneh, H.M. El-Kaderi, Exceptional gas adsorption properties by nitrogen-doped porous carbons derived from benzimidazole-linked polymers, *Chem. Mater.* 27 (2015) 1349–1358.
- [33] N. Ferrera-Lorenzo, E. Fuente, I. Suárez-Ruiz, B. Ruiz, Sustainable activated carbons of macroalgae waste from the agar-agar industry. Prospects as adsorbent for gas storage at high pressures, *Chem. Eng. J.* 250 (2014) 128–136.
- [34] X.H. Shao, Z.H. Feng, R.S. Xue, C.C. Ma, W.C. Wang, X. Peng, et al., Adsorption of CO<sub>2</sub>, CH<sub>4</sub>, CO<sub>2</sub>/N<sub>2</sub> and CO<sub>2</sub>/CH<sub>4</sub> in novel activated carbon beads: preparation, measurements and simulation, *AIChE J.* 57 (2011) 3042–3051.
- [35] D.P. Vargas, L. Giraldo, J.C. Moreno-Pirajan, Carbon dioxide and methane adsorption at high pressure on activated carbon materials, *Adsorption* 19 (2013) 1075–1082.
- [36] L.Y. Meng, S.J. Park, Influence of MgO template on carbon dioxide adsorption of cation exchange resin-based nanoporous carbon, *J. Colloid Interface Sci.* 366 (2012) 125–129.
- [37] S. Himeno, T. Komatsu, S. Fujita, High-pressure adsorption equilibria of methane and carbon dioxide on several activated carbons, *J. Chem. Eng. Data* 50 (2005) 369–376.
- [38] D.P. Bezerra, F.W.M. da Silva, P.A.S. de Moura, K. Sapag, R.S. Vieira, E. Rodriguez-Castellon, et al., Adsorption of CO<sub>2</sub> on amine-grafted activated carbon, *Adsorpt. Sci. Technol.* 32 (2014) 141–151.
- [39] P. Ning, F. Li, H. Yi, X. Tang, J. Peng, Y. Li, et al., Adsorption equilibrium of methane and carbon dioxide on microwave-activated carbon, *Sep. Purif. Technol.* 98 (2012) 321–326.
- [40] J.H. Cavka, C.A. Grande, G. Mondino, R. Blom, High pressure adsorption of CO<sub>2</sub> and CH<sub>4</sub> on Zr-MOFs, *Ind. Eng. Chem. Res.* 53 (2014) 15500–15507.
- [41] D. Saha, Z.B. Bao, F. Jia, S.G. Deng, Adsorption of CO<sub>2</sub>, CH<sub>4</sub>, N<sub>2</sub>O, and N<sub>2</sub> on MOF-5, MOF-177, and Zeolite 5A, *Environ. Sci. Technol.* 44 (2010) 1820–1826.
- [42] M. Hefti, D. Marx, L. Joss, M. Mazzotti, Adsorption equilibrium of binary mixtures of carbon dioxide and nitrogen on zeolites ZSM-5 and 13X, *Micro-porous Mesoporous Mater.* 215 (2015) 215–228.
- [43] Y.Y. Feng, W. Yang, W. Chu, K<sub>2</sub>S-activated carbons developed from coal and their methane adsorption behaviors, *Chin. Phys. B* 23 (2014) 108201–108208.
- [44] M. Elizabeth Casco, M. Martinez-Escandell, E. Gadea-Ramos, K. Kaneko, J. Silvestre-Albero, F. Rodriguez-Reinoso, High-pressure methane storage in porous materials: are carbon materials in the pole position? *Chem. Mater.* 27 (2015) 959–964.
- [45] W. Djeridi, A. Ouederni, A.D. Wiersum, P.L. Llewellyn, L. El Mir, High pressure methane adsorption on microporous carbon monoliths prepared by olives-stones, *Mater. Lett.* 99 (2013) 184–187.
- [46] A.A.G. Blanco, J.C.A. de Oliveira, R. Lopez, J.C. Moreno-Pirajan, L. Giraldo, G. Zgrablitch, et al., A study of the pore size distribution for activated carbon monoliths and their relationship with the storage of methane and hydrogen, *Colloids Surfaces Physicochem. Eng. Aspects* 357 (2010) 74–83.
- [47] M. Oschatz, L. Borchardt, I. Senkovska, N. Klein, M. Leistner, S. Kaskel, Carbon dioxide activated carbide-derived carbon monoliths as high performance adsorbents, *Carbon* 56 (2013) 139–145.
- [48] A. Aleghafouri, M. Mohsen-Nia, A. Mohajeri, M. Mahdyarfar, M. Asghari, Micropore size analysis of activated carbons using nitrogen, carbon dioxide and methane adsorption isotherms: experimental and theoretical studies, *Adsorpt. Sci. Technol.* 30 (2012) 307–316.
- [49] Y. Feng, W. Yang, N. Wang, W. Chu, D. Liu, Effect of nitrogen-containing groups on methane adsorption behaviors of carbon spheres, *J. Anal. Appl. Pyrolysis* 107 (2014) 204–210.
- [50] M.S. Balathanigaimani, W.G. Shim, J.W. Lee, H. Moon, Adsorption of methane on novel corn grain-based carbon monoliths, *Microporous Mesoporous Mater.* 119 (2009) 47–52.
- [51] J.S. Shi, W.B. Li, D. Li, Rapidly reversible adsorption of methane with a high storage capacity on the zeolite templated carbons with glucose as carbon precursors, *Colloids Surfaces Physicochem. Eng. Aspects* 485 (2015) 11–17.
- [52] R. Yang, G.Q. Liu, M. Li, J.C. Zhang, X.M. Hao, Preparation and N<sub>2</sub>, CO<sub>2</sub> and H<sub>2</sub> adsorption of super activated carbon derived from biomass source hemp (*Cannabis sativa* L.) stem, *Microporous Mesoporous Mater.* 158 (2012) 108–116.
- [53] Y.D. Xia, Z.X. Yang, Y.Q. Zhu, Porous carbon-based materials for hydrogen storage: advancement and challenges, *J. Mater. Chem. A* 1 (2013) 9365–9381.
- [54] M. Jordá-Beneyto, D. Lozano-Castello, F. Suarez-Garcia, D. Cazorla-Amorós, A. Linares-Solano, Advanced activated carbon monoliths and activated carbons for hydrogen storage, *Microporous Mesoporous Mater.* 112 (2008) 235–242.
- [55] J. Wang, I. Senkovska, S. Kaskel, Q. Liu, Chemically activated fungi-based porous carbons for hydrogen storage, *Carbon* 75 (2014) 372–380.
- [56] X. Liu, C. Zhang, Z. Geng, M. Cai, High-pressure hydrogen storage and optimizing fabrication of corn cob-derived activated carbon, *Microporous Mesoporous Mater.* 194 (2014) 60–65.
- [57] J. Zhu, J. Cheng, A. Dailly, M. Cai, M. Beckner, P.K. Shen, One-pot synthesis of Pd nanoparticles on ultrahigh surface area 3d porous carbon as hydrogen storage materials, *Int. J. Hydrogen Energy* 39 (2014) 14843–14850.
- [58] I. Wrobel-Iwaniec, N. Diez, G. Gryglewicz, Chitosan-based highly activated carbons for hydrogen storage, *Int. J. Hydrogen Energy* 40 (2015) 5788–5796.
- [59] M.C. Tellez-Juárez, V. Fierro, W. Zhao, N. Fernández-Huerta, M.T. Izquierdo, E. Reguera, et al., Hydrogen storage in activated carbons produced from coals of different ranks: effect of oxygen content, *Int. J. Hydrogen Energy* 39 (2014) 4996–5002.
- [60] W. Zhao, V. Fierro, N. Fernandez-Huerta, M.T. Izquierdo, A. Celzard, Impact of synthesis conditions of KOH activated carbons on their hydrogen storage capacities, *Int. J. Hydrogen Energy* 37 (2012) 14278–14284.
- [61] M.F.A. Aboud, Z.A. AL-Othman, M.A. Habila, C. Zlotea, M. Latroche, F. Cuevas, Hydrogen storage in pristine and d10-block metal-anchored activated carbon made from local wastes, *Energies* 8 (2015) 3578–3590.
- [62] Y. Xia, R. Mokaya, Ordered mesoporous carbon monoliths: CVD nanocasting and hydrogen storage properties, *J. Phys. Chem. C* 111 (2007) 10035–10039.
- [63] A. Almasoudi, R. Mokaya, Porosity modulation of activated ZIF-templated carbons via compaction for hydrogen and CO<sub>2</sub> storage applications, *J. Mater. Chem. A* 2 (2014) 10960–10968.
- [64] E. Masika, R. Mokaya, Preparation of ultrahigh surface area porous carbons templated using zeolite 13X for enhanced hydrogen storage, *Prog. Nat. Sci. Mater. Int.* 23 (2013) 308–316.
- [65] M.S. Balathanigaimani, W.G. Shim, T.H. Kim, S.J. Cho, J.W. Lee, H. Moon,

- Hydrogen storage on highly porous novel corn grain-based carbon monoliths, *Catal. Today* 146 (2009) 234–240.
- [66] Y.J. Heo, S.J. Park, Synthesis of activated carbon derived from rice husks for improving hydrogen storage capacity, *J. Ind. Eng. Chem.* 31 (2015) 330–334.
- [67] A.M. Silvestre-Albero, A. Wahby, J. Silvestre-Albero, F. Rodriguez-Reinoso, W. Betz, Carbon molecular sieves prepared from polymeric precursors: porous structure and hydrogen adsorption properties, *Ind. Eng. Chem. Res.* 48 (2009) 7125–7131.